

# The effect of inter-pass temperature on residual stresses in multi-pass welds produced using a low transformation temperature filler alloy

T. I. Ramjaun<sup>a</sup>, H. J. Stone<sup>a</sup>, L. Karlsson<sup>b</sup>, J. Kelleher<sup>c</sup>, R. J. Moat<sup>d</sup>, J. Rebelo Kornmeier<sup>e</sup>, K. Dalaei<sup>f</sup>,  
H. K. D. H. Bhadeshia<sup>a</sup>

<sup>a</sup>Materials Science and Metallurgy, University of Cambridge, CB2 3QZ, U.K.

<sup>b</sup>Engineering Science, University West, SE-461 86 Trollhättan, Sweden

<sup>c</sup>ISIS Facility, Rutherford Appleton Laboratory, Didcot, OX11 0QX, U.K.

<sup>d</sup>Materials Engineering, The Open University, Milton Keynes, MK7 6AA

<sup>e</sup>Technische Universität München, Forschungsneutronenquelle Heinz Maier-Leibnitz (FRM II), 85747 Garching, Germany

<sup>f</sup>ESAB AB, Lindholmsalvn 9, 417 55 Göteborg, Sweden

---

## Abstract

Weld filler alloys that exploit transformation plasticity through low austenite-to-martensite transformation temperatures offer an effective method of reducing residual stresses in strong, steel welds. However, in multi-pass welds the heat input from later weld passes may be insufficient to retransform prior welding passes, leading to the accumulation of thermally-induced strains and elevated residual stresses. In this work, the residual stress distributions produced around arc welds fabricated with a martensitic weld filler alloy that transforms at a low temperature, have been studied as a function of the number of passes deposited and the inter-pass temperature. It is found that when the inter-pass temperature is above the transformation temperature of the weld metal, the entire multi-pass weld transforms as a single entity, thus permitting the optimum exploitation of the transformation plasticity. In contrast, the deposition of new metal with a relatively low inter-pass temperature leads to increased residual stresses in the underlying layers, reducing or eliminating the beneficial stress states previously created.

*Keywords:* transformation induced plasticity, martensitic weld metal, residual stress, welding, phase transformation

---

## 1. Introduction

The residual stresses associated with welded joints are a problem in the optimum exploitation of engineering structures as they may compromise structural integrity and limit component life. One method by which such stresses may be mitigated, is through the use of a welding consumable that undergoes a displacive transformation at low temperatures. The plasticity associated with such transformations can compensate for the accumulated thermal contraction strains, thereby minimising or reversing the residual stresses that would otherwise develop. Based on the original work by Alberry and Jones [1], this has led to considerable research on the design of appropriate compositions [2–16], which have contributed to the development of this particular welding alloy.

---

*Email address:* tir20@cam.ac.uk (T. I. Ramjaun)

Recently, other compositions have also been investigated [17–22], the essential requirement of such weld filler alloys is that the phase transformation should not be exhausted until the weld cools to ambient temperature. Otherwise, further thermal contraction in the temperature range corresponding to the finish of transformation and room temperature will lead to increased stresses. In addition, phase changes that occur by a displacive process have a greater capacity for plasticity than those which require long-range diffusion. Both of these conditions favour the selection of a martensitic weld metal provided that the carbon concentration is kept low enough to avoid the embrittlement associated with hard martensite. The martensitic transformation is defined by a martensite-start temperature,  $M_S$ , and the temperature corresponding to  $\sim 95\%$  martensite, which is typically designated  $M_F$ . It therefore follows that  $M_F$  should be close to room temperature to minimise subsequent thermal strains and hence that  $M_S$  should be  $\sim 230^\circ\text{C}$ ; following the Koistinen and Marburger [23] equation. To achieve such a low martensite-start temperature while limiting the carbon concentration requires the weld metal to contain relatively large concentrations of solute such as nickel and chromium, so it is not surprising that the total substitutional alloying element concentration in low transformation temperature (LTT) weld filler alloys is usually 15–20 wt% [16].

Diffraction data and fatigue tests have demonstrated that the use of LTT weld filler alloys can be beneficial in mitigating residual stresses and their consequences [2, 3, 6, 13, 24–28]. However, there may be difficulties in applying the concept to multi-pass welds in which the deposit is built up in layers in order to fill the weld joint. In such circumstances, much of the LTT material deposited first will not be reheated into the austenitic phase by the heat of a subsequent layer and therefore thermally-induced strains will accumulate, which will be retained to room temperature.

A possible way of avoiding this issue is through the use of an inter-pass temperature in excess of  $M_S$ . This enables the whole of the multi-layer, filled weld joint to remain austenitic. On subsequent cooling at the end of the welding operation the entire deposit can then transform into martensite in order to cancel the development of contraction stresses. The process is illustrated in Fig. 1. In the present work, neutron diffraction has been performed on single and multi-pass welds fabricated with a LTT weld filler alloy to assess the effect of inter-pass temperatures,  $T_i$ , relative to  $M_S$  on the residual stress distributions produced.

## 2. Experimental Method

Welds were prepared on plates of the commercially available high strength steel, Weldox 700, using a martensitic stainless steel filler alloy with a low  $M_S$ , LTT-1 [15]. The compositions of both of these alloys are shown in Table 1. The martensite-start temperature of the LTT filler alloy was measured using dilatometry on cylindrical samples of length 12 mm and diameter 8 mm cut from a 20 mm thick 18-pass buttered butt-weld to minimise dilution, with the data analysed according to [29]. Using this method, the martensite start temperature was determined to be  $164 \pm 12^\circ\text{C}$ .

Automated gas-shielded metal arc welding (GMAW) was performed on four identical Weldox 700 plates of dimensions  $500 \times 150 \times 15$  mm, machined with  $60^\circ$  V-grooves, each with a root radius of 4 mm, Fig. 2. The plates were clamped to the bench prior to welding, which was performed horizontally in the down hand position; the welding parameters and number of layers deposited are listed in Tables 2–3. To ascertain the extent of stress relief that can be achieved with the LTT filler alloy, one, single-pass weld (weld A) was prepared. Three further three-pass welds were subsequently fabricated with different inter-pass temperatures (welds B,C,D) from which the effect of multiple welding passes and inter-pass temperature on the residual stress distributions produced could be determined.

## 2.1. Neutron Diffraction

The residual stresses in the welded plates were measured using neutron diffraction [30] on two strain scanning instruments: the STRESS-SPEC beamline [31] at the FRM II reactor (weld C & D), and the ENGIN-X beamline [32] at the ISIS pulsed spallation neutron source (weld A & B). For both experiments, strain scanning was performed across a plane perpendicular to the weld at the position along the sample shown in Fig. 3a. Measurements were made across both sides of the weld, heat-affected zone (HAZ) and extended into the base plate to identify any asymmetry in the stress field. It was assumed that the principal stresses are parallel to the plate edges.

The STRESS-SPEC measurements were made using a monochromatic beam with a wavelength of  $\sim 1.69 \text{ \AA}$ , provided from a bent Si (400) monochromator set to a take off angle  $2\theta_M = 77.3^\circ$ . The diffracted intensities were recorded on a  $30 \times 30 \text{ cm}^2$  position-sensitive detector. Measurements of the  $\{211\}$  ferrite diffraction peak were performed around a scattering angle of  $2\theta_S \approx 92.5^\circ$ . The  $\{211\}$  peak was selected as this reflection is known to accumulate only small compressive intergranular stresses following uniaxial tensile deformation [33, 34]. The stresses determined from the strains measured with this reflection and the appropriate diffraction elastic constant were therefore taken to be representative of the macroscopic residual stress. A gauge volume of  $2 \times 2 \times 2 \text{ mm}^3$  was defined by a primary slit of  $2 \times 2 \text{ mm}^2$  and a secondary 2 mm radial collimator for the longitudinal direction. The transverse and normal directions were measured using a gauge volume  $2 \times 20 \times 2 \text{ mm}^3$ , with the long dimension of this volume parallel to the weld direction. The use of an elongated gauge volume in the welding direction was deemed appropriate as the residual stress is not expected to vary significantly along the central portion of the welded plates.

The ENGIN-X beam line uses time-of-flight neutron diffraction to measure a continuous range of reciprocal space at  $2\theta_M$  angles from  $76\text{-}104^\circ$ . The inter-planar spacings of many different reflections are thus recorded simultaneously. A single macroscopic strain value was found for each measured location and direction using the lattice parameter derived from a Pawley fit to the measured diffraction data. This approach has been shown to be effective in providing a measure of the average residual strains and may be directly converted to stress using the appropriate bulk values of the elastic constants [35]. Following the approach described above for the STRESS-SPEC measurements, a  $3 \times 3 \times 3 \text{ mm}^3$  gauge volume was used for the longitudinal strain measurements, and  $3 \times 15 \times 3 \text{ mm}^3$  used for the transverse and normal strain measurements. Again, a fixed 3 mm radial collimator was used to define one dimension of the gauge volume, with the other two defined by the cross-section of the incident beam.

## 2.2. Stress Analysis

In order to determine the residual stresses across the welded plates, strain-free reference specimens were used to account for the effect of compositional variation between the filler alloy and base plate on the measured lattice spacings, which would otherwise be misinterpreted as strain. These were removed as 3 mm thick cross-sectional slices from the welded plate, as shown in Fig. 3a, and further slotted at 3 mm intervals along the transverse direction using wire electro-discharge machining, Fig. 3b, to form a ‘comb’ sample typically used for this type of work [36].

From the STRESS-SPEC data, the elastic strain,  $\varepsilon_{hkl}$ , at each measurement location and direction was found from a comparison of the measured lattice spacing in the weld,  $d_{hkl}$ , for a reflection  $(hkl)$  to that at the corresponding location in the stress-free reference sample,  $d_{0,hkl}$ :

$$\varepsilon_{hkl} = \frac{d_{hkl} - d_{0,hkl}}{d_{0,hkl}} \quad (1)$$

Elastic strains were calculated from the ENGIN-X data in an analogous way using the lattice parameters obtained from the Pawley fits.

The stress,  $\sigma_{ii}$ , in each of the three orthogonal directions was found from the strain measurements according to:

$$\sigma_{ii} = \frac{E}{(1 + \nu)} \left[ \varepsilon_{ii} + \frac{\nu}{(1 - 2\nu)} (\varepsilon_{11} + \varepsilon_{22} + \varepsilon_{33}) \right] \quad (2)$$

where  $E$  is the Young's modulus and  $\nu$  is Poisson's ratio.  $E = 220$  GPa and  $\nu = 0.28$  are the diffraction elastic constants for the  $\{211\}$  used to calculate the stress in welds C and D [37].  $E = 212.7$  GPa and  $\nu = 0.30$  are the macroscopic bulk properties for a ferritic steel following the Kröner model and used to calculate the stress in welds A and B [38].  $i = 1, 2, 3$  denotes the direction of the initial lattice parameter of lattice spacing measurement and hence, strain and stress direction with respect to the welded plate geometry. Linear interpolation of the data obtained from the comb sample allowed suitable strain free reference inter-planar spacings or lattice parameters to be obtained for each measurement position in the welded plate. Although shear stresses were not measured in this coordinate system, Equation 2 remains valid even when the orthogonal directions are not the principal directions. In practice, one would expect that the longitudinal direction is a principal direction, but that the other two principal directions may vary on the plane normal to the longitudinal axis.

### 3. Results and Discussion

#### 3.1. Residual Stress Measurements

The residual stress measurements are presented as stress contours overlaid on their respective macrographs for the longitudinal, transverse and normal directions for each of the four welded plates, Fig. 4. The crosses represent the original strain measurement positions and the stress contours have been restricted to the minimum (2.5 mm) and maximum (12.5 mm) measurement positions below the surface; extrapolation to the surface would not be appropriate due to potentially steep stress gradients that would need to be taken into account. It is noted that the measured stresses are averaged over a the gauge volume which represents the spatial resolution of the technique used. This will have the effect of smoothing variations, particularly where the gradients are steep. Consistent with the weld geometry, the stress contours show remarkable symmetry reflected across the weld centreline. The contours, as expected, follow the fusion surface, as has been seen in similar experiments [10].

Compressive stresses can be seen in the weld material for all four specimens in both the longitudinal and transverse directions, providing comprehensive evidence for the shape deformation and net expansion of these types of low transformation temperature alloys [39]. The stresses accumulated in the welded plates are greatest in the longitudinal direction. This is to be expected as this is the direction of maximum thermal constraint during cooling. In all four welded plates the longitudinal stresses show a general trend of compression being developed within the weld metal, which decreases in magnitude and reverses sign as the measurement position moves towards the heat affected zone. This occurs on either side of or below the weld metal in the base plate due to the equilibration of stress and the absence of transformation plasticity in these regions. The same stress distribution is evident for the transverse direction.

In all welds the peak tensile longitudinal residual stresses are of the order of  $\sim 600$  MPa and are observed in the heat affected zone. In contrast, within the fusion zones of all welds compressive longitudinal stresses are seen in the range -200 to -400 MPa. Whilst the largest stresses occur in the longitudinal direction, significant stresses were also measured in the transverse direction. As with the longitudinal stresses, the largest tensile transverse stresses are observed in the heat affected zone and are up to 400 MPa, whilst compressive transverse stresses up to -200 MPa are seen in the weld bead. The range of stresses developed in the normal direction are much lower, being  $\sim 300$  MPa in the base plate and  $\sim -100$  MPa in the weld bead, but follow a similar pattern of stress distribution as the longitudinal and transverse directions.

More detail can be seen in the longitudinal-stress profiles presented in Figs. 5–8, which show the residual stresses at exact locations within the welded plate (rather than smoothed contours) and further

highlight the symmetry about the weld centreline. These are discussed in more detail in the section that follows.

### 3.2. The Effects of Inter-pass Temperature

The longitudinal stress profile for the single-pass weld, weld A, Fig. 5, shows compressive residual stresses of  $\sim -300$  MPa generated in the weld metal at a depth of 7.5 mm. As subsequent layers of filler are deposited, the same position records a zero residual stress state. This can be seen in the data presented for weld B in Fig. 6. This suggests that the deposition of one layer on to another does not sufficiently austenitise the underlying deposit to regenerate the stress-relief due to transformation plasticity. This phenomenon is also evident for weld C, where the sign of the longitudinal stress at a depth of 7.5 mm is reversed so that the material at that location is left with a large tensile stress of  $\sim 600$  MPa, as can be seen in Fig. 7. It is notable, however, that the results obtained from weld D shown in Fig. 8 do not fit into this trend with compressive stress surviving the creation of a multi-pass deposit. An examination of Fig. 4 shows that the transverse stresses in welds A, B and C show the same, though less pronounced, changes from compression to tensile stress in the weld metal when additional weld layers are deposited.

Welds C and D, although being identical in geometry and composition, show profoundly different residual stress distributions: *cf.* Figs 4, 7, 8. The large compressive stress of  $\sim -400$  MPa in the weld bead of weld C at a depth of 5 mm at the weld centreline changes abruptly into a large tensile stress of about 600 MPa at 7.5 mm, for which the measurement position was largely within the first layer of the weld material. The compressive stress in weld D is comparatively lower in magnitude, being  $\sim -200$  MPa, but covers a much larger region and remains in compression at 7.5 mm. These differences in stress distribution are a consequence of the selected inter-pass temperatures with respect to the  $M_S$  temperature (Table 3). Given that the weld metal  $M_S$  temperature is  $M_S = 164 \pm 12$  °C, in the case of weld C, the inter-pass temperature was always below  $M_S$  at 45-50°C so that following deposition, each layer transforms into martensite before another is deposited. Therefore, only those regions of the first layer which happen to reaustenitise due to the heat from the subsequent layer can contribute to transformation plasticity; the remainder of the first layer simply contributes to constraint and accumulates thermally-induced strains. The beneficial stress system introduced when the first layer was deposited, is therefore lost or reduced.

In contrast, the inter-pass temperature in the case of weld D was kept in the range 200-240°C, so that the weld metal should remain fully austenitic, only to form martensite after all layers are deposited and the welded plate is finally allowed to cool below  $M_S$ . The martensitic transformation of the entire weld then ensures that the benefits of transformation plasticity are optimally exploited, thus resulting in a persistent compression at the weld centreline. The fact that weld D does indeed remain largely austenitic is clear from the images presented in Fig. 9-10. The columnar austenite grains terminate at layer junctions in weld C, whereas they are continuous across the second and third layers in the case of weld D. This is a classic replication of the effect observed when welding austenitic stainless steels, where the lengthy columnar grains extend completely across welds by epitaxial growth since no nucleation is needed when subsequent layers are deposited [40].

On a thermodynamic basis, the first solid to form is  $\delta$ -ferrite and this is then replaced by columnar austenite grains [41], but for the alloys of interest, solidification usually consists of a mixture of  $\delta$ -ferrite and austenite at the fusion surface [42, Chapter 9]. When the inter-pass temperature is high so that the substrate consists of columnar austenite grains, the increase in temperature due to the deposition of a subsequent layer leads to the formation some  $\delta$ -ferrite, but the original austenite grains continue to grow and eventually consume the  $\delta$ -ferrite, thus leading to a continuity of  $\gamma$  grains across beads. In contrast, when an inter-pass temperature below the  $M_S$  is implemented, new austenite grains are generated during heating, thus destroying any possibility of  $\gamma$ -continuity across beads. It should be noted, that the  $M_S$  of the first deposited layer will be higher than subsequent layers by virtue of compositional dilution with the base plate. This could reduce the alloying additions in the weld metal up to 30% and increase the  $M_S$

to  $\sim 240^\circ\text{C}$ , the inter-pass temperature for weld D. If the  $M_S > T_I$ , continuity of columnar grains across the fusion boundary into the second layer will not occur. However, the  $M_S$  is in very close proximity to the  $T_I$  so that the majority of the first pass will remain as untransformed  $\gamma$  until all three layers have been deposited and transformation to martensite occurs with final cooling; this is indicated by the residual stress contours. In order to maintain a more uniform  $M_S$  across the multi-pass weld, a more highly alloyed weld filler should be used for the first layer. Indeed, dilution will occur with the deposition of each new layer, causing a variation in the  $M_S$ , but it is most significant for the first layer and reduces with the number of passes.

There is a good correlation between the changes in the longitudinal stress profiles across welds B, C and D (Figs. 6-8) and their varying inter-pass temperatures. Weld C ( $T_I \approx 50^\circ\text{C}$ ) shows compressive residual stresses of around  $-500\text{ MPa}$  in the weld material at depths of 2.5 and 5.0 mm along the weld centreline, which change abruptly to a large tensile stress of  $\sim 600\text{ MPa}$  at a depth 7.5 mm and remains tensile with increasing depth into the base plate. Weld B ( $T_I \approx 120^\circ\text{C}$ ), displays slightly less extreme stress values in the weld material but the profiles follow the same trend as for weld C, the only difference being the zero stress value recorded at 7.5 mm depth. As the inter-pass temperature is raised above the  $M_S$  in weld D ( $T_I \approx 240^\circ\text{C}$ ) the stress at 7.5 mm depth becomes compressive, being  $\sim -300\text{ MPa}$ , and the value at 10 mm depth falls to below  $150\text{ MPa}$ . Weld C has an inter-pass temperature sufficiently below the  $M_S$  to cause each individual welding pass to transform to martensite prior to the next layer being deposited. Weld D has a sufficiently high inter-pass temperature such that all passes transformed collectively. Weld B, with an intermediary inter-pass temperature displays stress profiles between the two extremes, this is explained by the transformation of austenite to martensite occurring over a temperature range [23] rather than at an absolute value. Applying an inter-pass temperature between  $M_S$  and  $M_F$  permits the formation of some martensite, which will be tempered by the subsequent welding pass and contribute towards improved toughness.

#### 4. Conclusions

- A low transformation-temperature welding alloy has been shown to be capable of inducing compressive residual stresses in the weld metal of both single- and multi-pass welds.
- Compressive stresses developed in the first welding pass can be eradicated by the deposition of additional layers if the majority of the underlying weld material is not austenitised by the heat input of the new layer.
- If the inter-pass temperature is maintained above the  $M_S$  for all welding passes, the entire weld remains austenitic until all the layers have been deposited. It therefore becomes possible to gain the stress reduction benefits that can be derived from the transformation plasticity of each and every layer.
- A more highly alloyed weld filler should be used for the first deposited layer to compensate for dilution with the base material and maintain a uniform  $M_S$  across all welding layers.
- Steep stress gradients exist across the weld, especially at fusion boundaries. This may necessitate a smaller gauge volume and an increased concentration of measurement points in these regions to accurately determine the abrupt changes in stress for these types of experiments.

#### Acknowledgments

We are grateful to ESAB AB for sponsoring this research. We also acknowledge the support of Dr. Ivan Lonardelli for his participation in the experimental team. This work is based upon experiments performed on the ENGIN-X instrument at

ISIS, Rutherford Appleton Laboratory, Didcot, U.K. and the STRESS-SPEC instrument operated by FRM II at the Heinz Maier-Leibnitz Zentrum (MLZ), Garching, Germany.

## References

- [1] W. K. C. Jones, P. J. Alberry: *Metals Technology* 11 (1977) 557–566.
- [2] A. Ohta, N. Suzuki, Y. Maeda, K. Hiraoka, T. Nakamura: *International Journal of Fatigue* 21 (1999) S113–S118.
- [3] A. Ohta, O. Watanabe, K. Matsuoka, C. Shiga, S. Nishijima, Y. Maeda, N. Suzuki, T. Kubo: *Welding in the World* 43 (1999) 38–42.
- [4] P. J. Withers, H. K. D. H. Bhadeshia: *Materials Science and Technology* 17 (2001) 355–365.
- [5] P. J. Withers, H. K. D. H. Bhadeshia: *Materials Science and Technology* 17 (2001) 366–375.
- [6] A. Ohta, K. Matsuoka, N. T. Nguyen, Y. Maeda, N. Suzuki: *Welding Journal, Research Supplement* 82 (2003) 77s–83s.
- [7] J. Eckerlid, T. Nilsson, L. Karlsson: *Science and Technology of Welding and Joining* 8 (2003) 353–359.
- [8] H. Lixing, W. Dongpo, W. Wenxian, Y. Tainjin: *Welding in the World* 48 (2004) 34–39.
- [9] S. Zenitani, N. Hayakawa, J. Yamamoto, K. Hiraoka, Y. Morikage, T. Yauda, K. Amano: *Science and Technology of Welding and Joining* 12 (2007) 516–522.
- [10] J. A. Francis, H. J. Stone, S. Kundu, R. B. Rogge, H. K. D. H. Bhadeshia, P. J. Withers, L. Karlsson: Transformation temperatures and welding residual stresses in ferritic steels: in: *Proceedings of PVP2007, ASME Pressure Vessels and Piping Division Conference: American Society of Mechanical Engineers: ASME, San Antonio, Texas, 2007: pp. 1–8.*
- [11] P. P. Darcis, H. Katsumoto, M. C. Payares-Asprino, S. Liu, T. A. Siewert: *Fatigue and Fracture of Engineering Materials and Structures* 31 (2008) 125–136.
- [12] M. C. Payares-Asprino, H. Katsumoto, S. Liu: *Welding Journal, Research Supplement* 87 (2008) 279s–289s.
- [13] H. Dai, J. A. Francis, H. J. Stone, H. K. D. H. Bhadeshia, P. J. Withers: *Metallurgical & Materials Transactions A* 39 (2008) 3070–3078.
- [14] Y. Mikami, Y. Morikage, M. Mochizuki, M. Toyoda: *Science and Technology of Welding and Joining* 14 (2009) 97–105.
- [15] A. A. Shirzadi, H. K. D. H. Bhadeshia, L. Karlsson, P. J. Withers: *Science and Technology of Welding and Joining* 14 (2009) 559–565.
- [16] R. J. Moat, H. J. Stone, A. A. Shirzadi, J. A. Francis, S. Kundu, A. F. M. H. K. D. H. Bhadeshia, L. Karlsson, P. J. Withers: *Science and Technology of Welding and Joining* 16 (2011) 279–284.
- [17] A. Kromm, T. Kannengiesser: *Welding in the World* 55 (2011) 48–56.
- [18] O. Özdemir, G. Çam, H. Çimenoglu, M. Koçak: *International Journal of Surface Science and Engineering* 6 (2012) 157–173.
- [19] J. Altenkirch, J. Gibmeier, A. Kromm, T. Kannengiesser, T. Nitschke-Pagel, M. Hofmann: *Materials Science and Engineering A* 528 (2011) 5566–5575.

- [20] J. Altenkirch, J. Gibmeier, V. Kostov, A. Kromm, T. Kannengiesser, S. Doyle, A. Wanner: *Journal of Strain analysis* 46 (2011) 563–579.
- [21] A. Kundu, P. J. Bouchard, S. Kumar, K. A. Venkata, J. A. Francis, A. Paradowska, G. K. Dey, C. E. Truman: *Science and Technology of Welding and Joining* 18 (2012) 70–75.
- [22] M. J. Xu, H. Lu, C. Yu, J. J. Xu, J. M. Chen: *Science and Technology of Welding and Joining* 18 (2013) 184–190.
- [23] D. P. Koistinen, R. E. Marburger: *Acta Metallurgica* 7 (1959) 59–60.
- [24] J. A. Francis, M. Turski, P. J. Withers: *Materials Science and Technology* 25 (2009) 325–334.
- [25] J. A. Francis, H. J. Stone, S. Kundu, R. B. Rogge, H. K. D. H. Bhadeshia, P. J. Withers, L. Karlsson: *Journal of Pressure Vessel Technology* 131 (2009) 0414011–0414018.
- [26] L. Karlsson, L. Mráz, H. K. D. H. Bhadeshia, A. Shirzadi: *Biuletyn Instytutu Spawalnictwa* 5 (2010) 33–39.
- [27] XV ESAB welding seminar: Increasing fatigue life with low transformation temperature (LTT) welding consumables.
- [28] K. T. C. Miki, T. Hanji: *Welding in the World* 56 (2012) 40–50.
- [29] H.-S. Yang, H. K. D. H. Bhadeshia: *Materials Science and Technology* 23 (2007) 556–560.
- [30] M. E. Fitzpatrick, A. Lodini (Eds.): *Analysis of Residual Stress by Diffraction using Neutron and Synchrotron Radiation*: CRC Press, Florida, USA, 2003.
- [31] M. Hofmann, G. A. Seidl, J. R. Kornmeier, U. Garde, R. Schneider, R. C. Wimpory, U. Wasmuth, U. Noster: *Materials Science Forum* 524–525 (2006) 211–216.
- [32] J. R. Santisteban: *Journal of Applied Crystallography* 39 (2006) 812–825.
- [33] M. R. Daymond, H. G. Priesmeyer: *Acta Materialia* 50 (2002) 1613–1626.
- [34] J. W. L. Pang, T. M. Holden, T. E. Mason: *Journal of Strain Analysis for Engineering Design* 33 (1998) 373–383.
- [35] M. R. Daymond, M. A. M. Bourke, R. B. V. Dreele, B. Clausen, T. Lorentzen: *Journal of Applied Physics* 82 (1997) 1554–1562.
- [36] P. J. Withers, M. Preuss, A. Steuwer, J. W. L. Pang: *Journal of Applied Crystallography* 40 (2007) 891–904.
- [37] B. Eigenmann, E. Macherauch: *Materialwissenschaft und Werkstofftechnik* 27 (1996) 426–437.
- [38] M. T. Hutchings, P. J. Withers, T. M. Holden, T. Lorentzen: *Introduction to the Characterization of Residual Stress by Neutron Diffraction*: Taylor & Francis, 2005.
- [39] H. K. D. H. Bhadeshia, J. A. Francis, H. J. Stone, S. Kundu, R. B. Rogge, P. J. Withers, L. Karlsson: Transformation plasticity in steel weld metals: in: *Proceedings of the 10th International Aachen Welding Conference*: Aachen University, Germany, 2007: pp. 22–25.
- [40] N. H. Tyas: Grain refinement of austenitic stainless steel welds to facilitate ultrasonic inspection: Ph.D. thesis: University of Cambridge: Cambridge, U. K. (2000).

- [41] H. K. D. H. Bhadeshia, L.-E. Svensson: Modelling the evolution of microstructure in steel weld metals: in: H. Cerjak, K. E. Easterling (Eds.), *Mathematical Modelling of Weld Phenomena: Vol. 1*: The Institute of Materials, London, 1993: pp. 109–182.
- [42] S. Kou: *Welding Metallurgy*: Wiley-Interscience, New Jersey, USA, 2002.

Table 1: Compositions (wt%) of the undiluted welding alloy and base plate.

Material	C	Si	Mn	Cr	Ni	Mo
LTT-1	0.01-0.03	0.6-0.8	1.2-1.7	12.5-13.0	5.5-6.5	<0.1
Weldox 700	0.25	0.29	0.98	0.25	0.043	0.15

Table 2: Welding parameters.

Wire type	Shielding gas	Gas flow ( $l\ min^{-1}$ )	Heat input ( $kJ\ mm^{-1}$ )	Voltage (V)	Current (A)	Welding speed ( $cm\ s^{-1}$ )
Metal-cored	Ar+2%CO <sub>2</sub>	18	$\approx 1.0$	24.7	$\approx 250$	23-36

Table 3: Pre-heat and inter-pass temperatures ( $T_I$ ). For the purposes of the present work we do not distinguish between the preheat and inter-pass temperatures.

Temperature ( $^{\circ}C$ )	Weld A	Weld B	Weld C	Weld D
Pre-heat	55	55	45	200
Inter-pass (1st-2nd layer)	—	115	50	240
Inter-pass (2st-3rd layer)	—	125	49	240

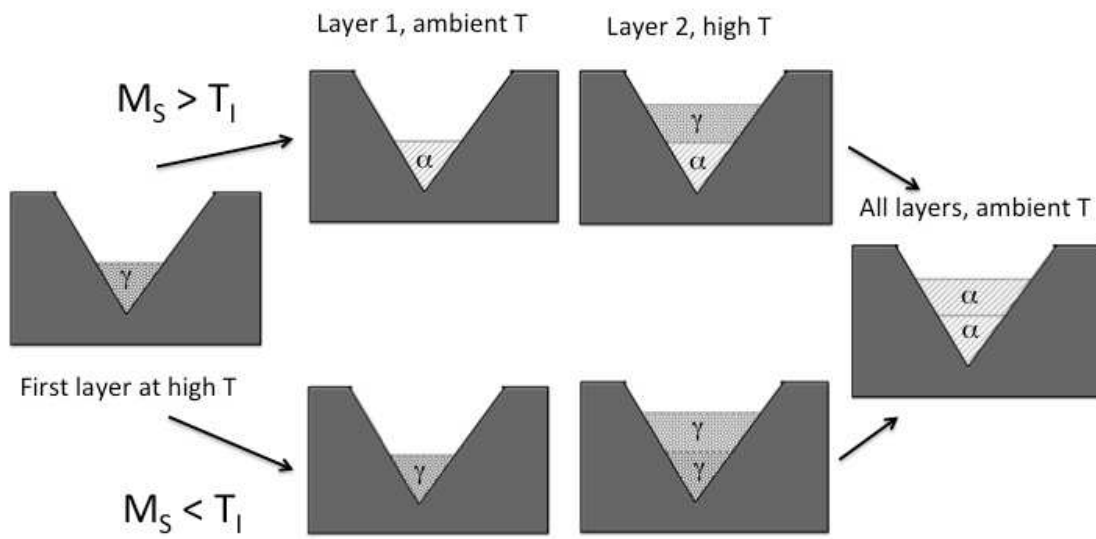


Figure 1: The influence of the difference between the inter-pass temperature  $T_I$  and the  $M_S$  temperature on the development of structure in the weld. When  $M_S > T_I$ , the multilayer weld does not transform homogeneously, whereas for  $M_S < T_I$ , all the layers remain austenitic until the weld is completed. Note that partial austenitisation that is likely for  $M_S > T_I$  is not illustrated for the sake of clarity.

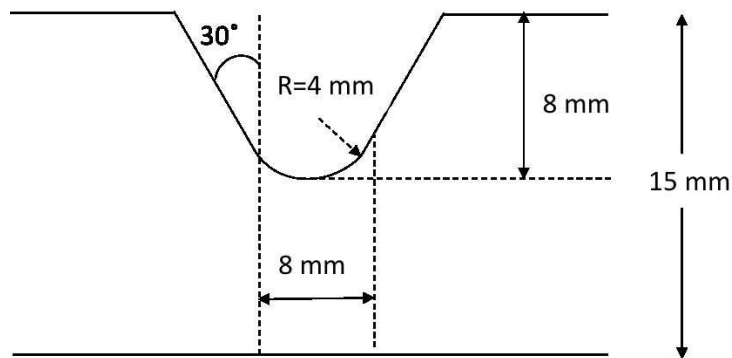


Figure 2: Cross-section of the machined V-groove, cut along the length of the plate prior to welding.

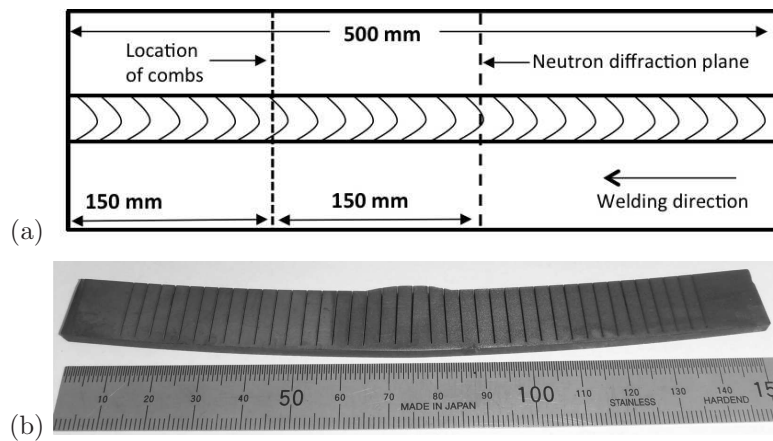


Figure 3: (a) Plan view of a welded plate showing the locations of the residual strain measurements and reference strain-free specimens. (b)Sectioned specimen used to determine the strain-free lattice parameter.

Science and Technology of Welding and Joining 19 (2014) 44-51

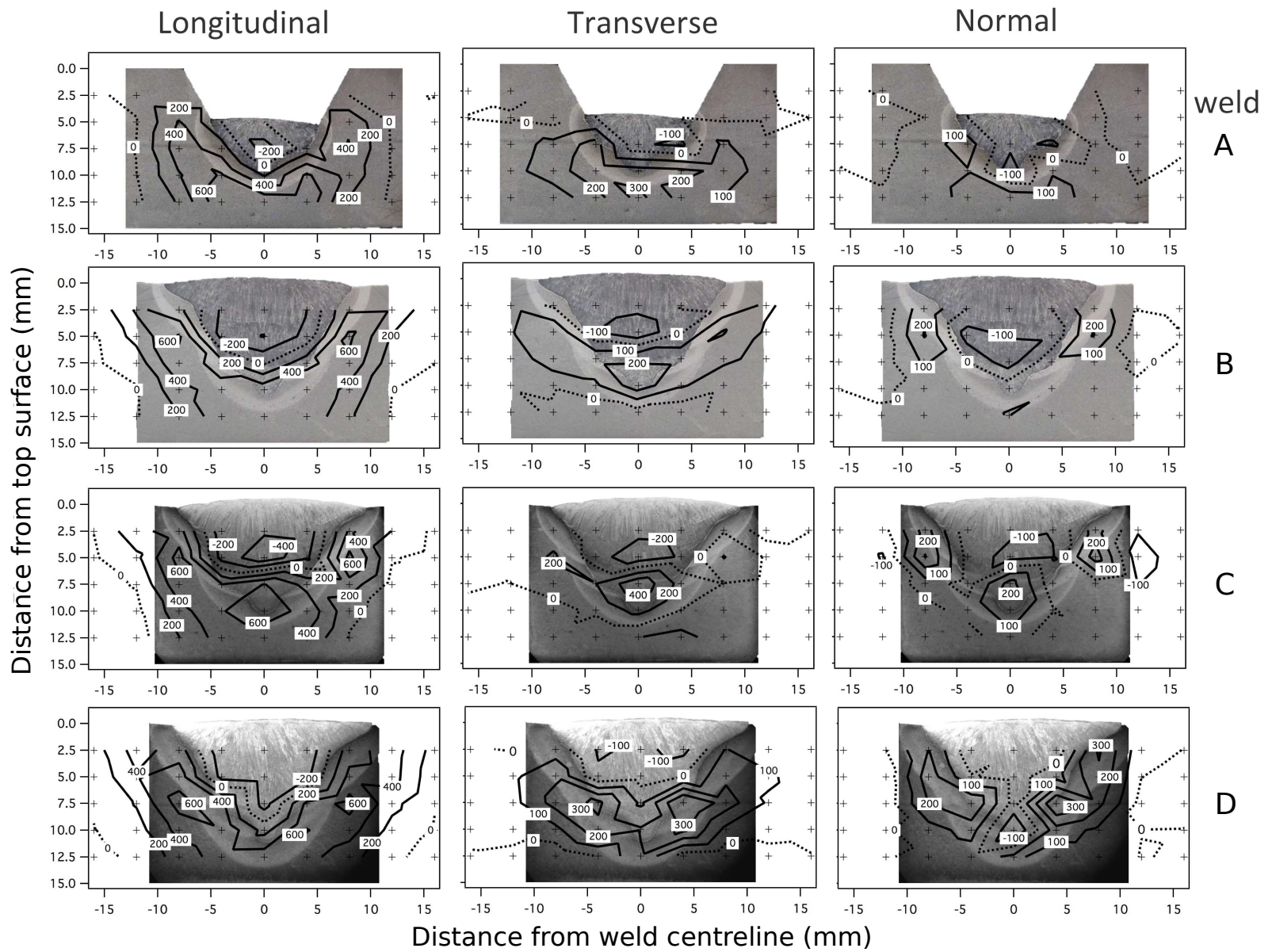


Figure 4: Residual stress contours in MPa, for the four different welds.

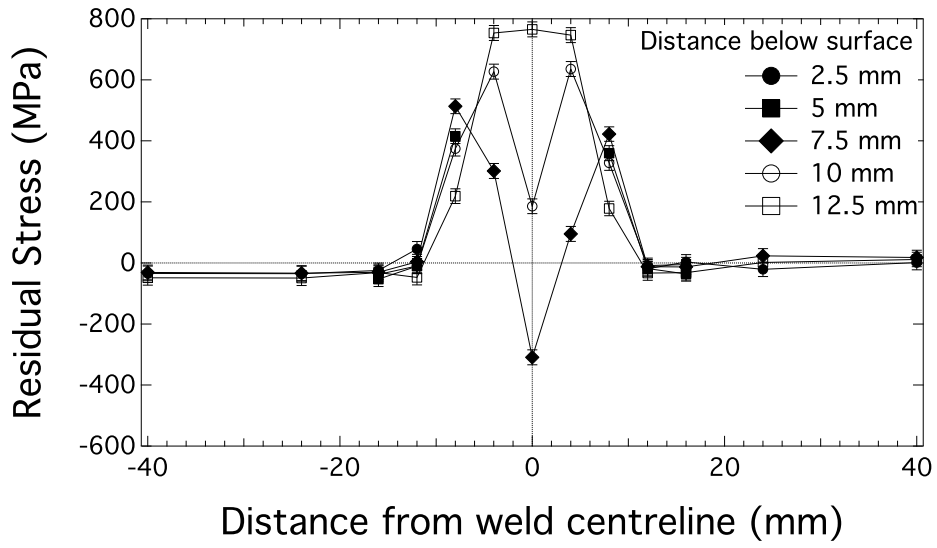


Figure 5: Longitudinal residual stress profiles as a function of distance from the weld centreline – Weld A

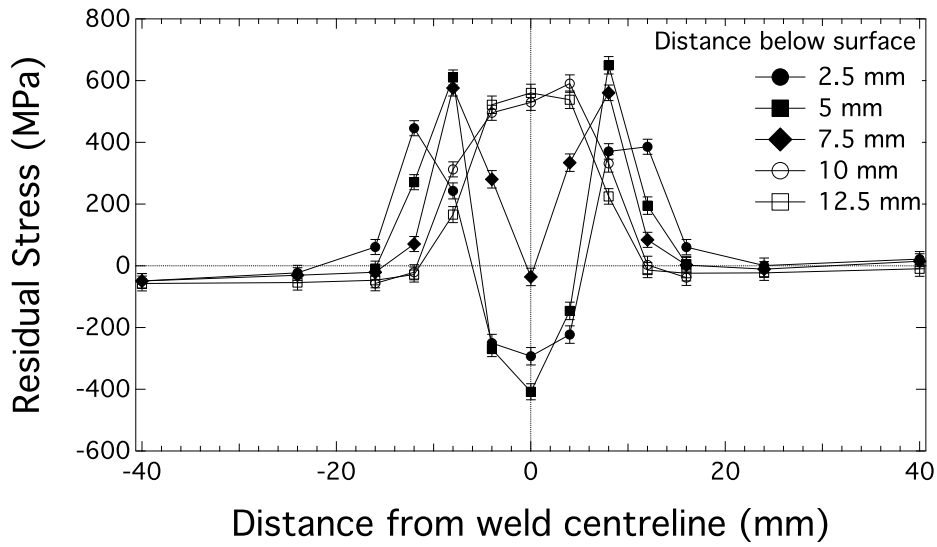


Figure 6: Longitudinal residual stress profiles as a function of distance from the weld centreline – Weld B

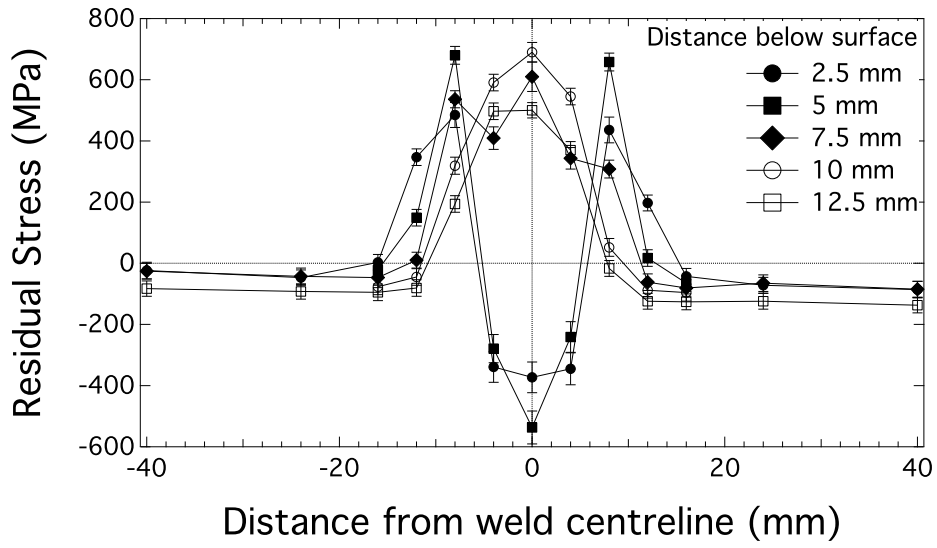


Figure 7: Longitudinal residual stress profiles as a function of distance from the weld centreline – Weld C

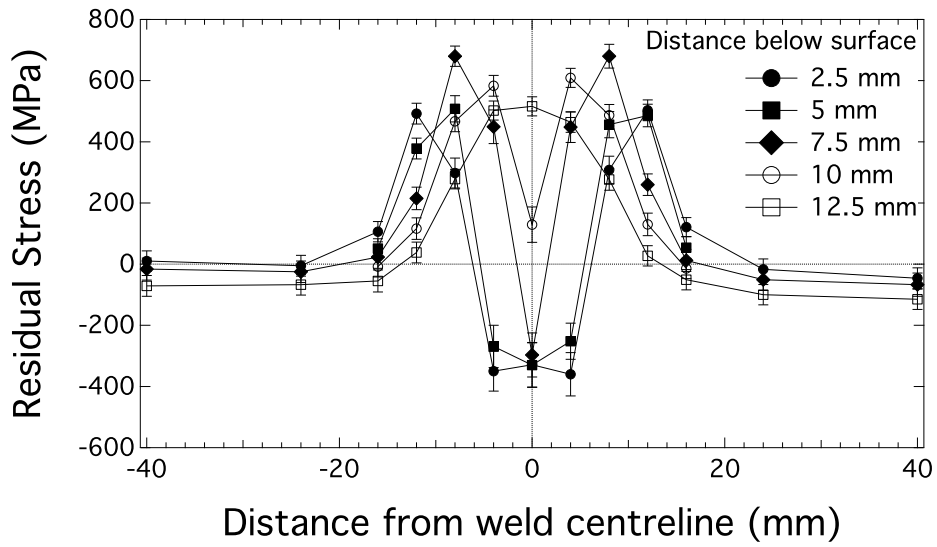


Figure 8: Longitudinal residual stress profiles as a function of distance from the weld centreline – Weld D

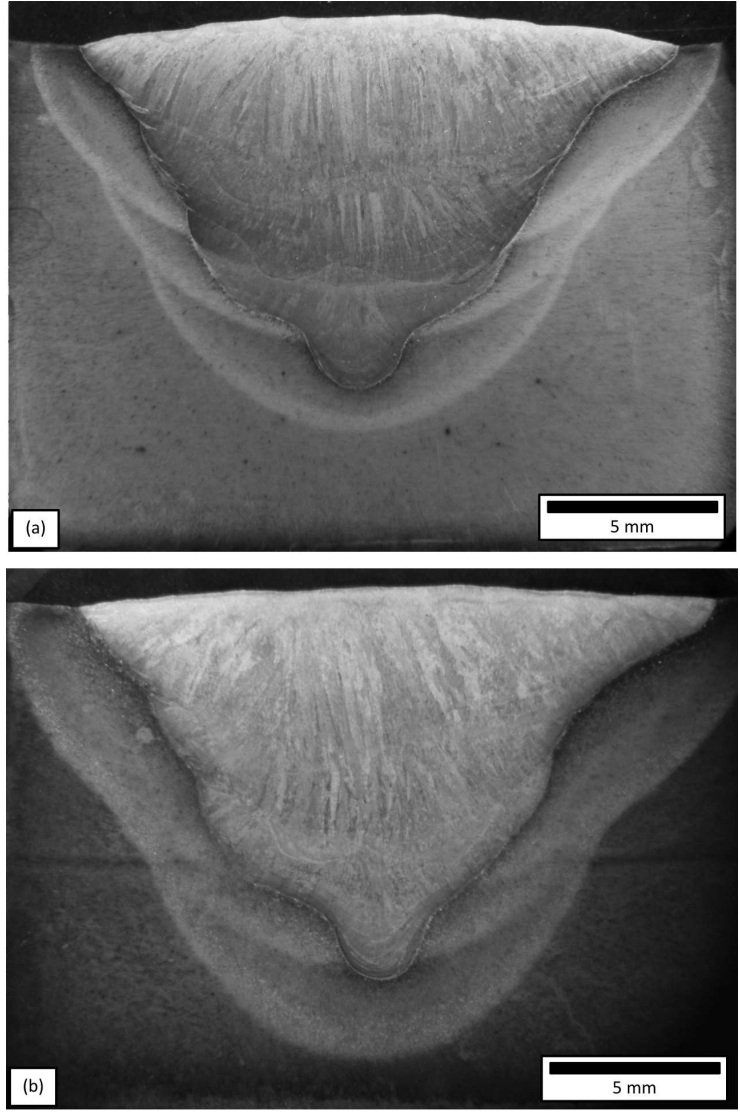


Figure 9: Macrostructures of (a) weld C, (b) weld D revealed using ferric chloride.

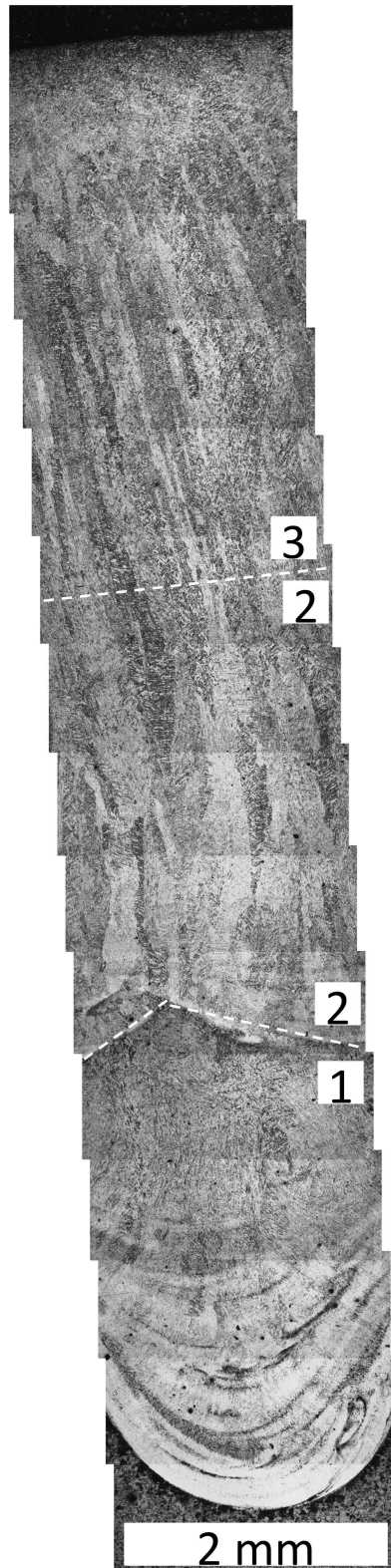


Figure 10: Microstructure of weld D at the centreline, from the weld root to the top surface highlighting the boundaries between layers.